



ELSEVIER

Available online at www.sciencedirect.com



Remote Sensing of Environment xx (2007) xxx–xxx

Remote Sensing  
of  
Environment

www.elsevier.com/locate/rse

## Evaluation of hyperspectral data for pasture estimate in the Brazilian Amazon using field and imaging spectrometers

Izaya Numata <sup>a,\*</sup>, Dar A. Roberts <sup>a</sup>, Oliver A. Chadwick <sup>a</sup>, Joshua P. Schimel <sup>b</sup>,  
Lênio S. Galvão <sup>c</sup>, João V. Soares <sup>c</sup>

<sup>a</sup> Department of Geography, University of California, Santa Barbara, CA 93106, USA

<sup>b</sup> Department of Ecology, Evolution, and Marine Biology, University of California Santa Barbara, CA 93106, USA

<sup>c</sup> Instituto Nacional de Pesquisas Espaciais, São José dos Campos, SP, Brazil

Received 13 October 2006; received in revised form 27 July 2007; accepted 14 August 2007

### Abstract

We used two hyperspectral sensors at two different scales to test their potential to estimate biophysical properties of grazed pastures in Rondônia in the Brazilian Amazon. Using a field spectrometer, ten remotely sensed measurements (i.e., two vegetation indices, four fractions of spectral mixture analysis, and four spectral absorption features) were generated for two grass species, *Brachiaria brizantha* and *Brachiaria decumbens*. These measures were compared to above ground biomass, live and senesced biomass, and grass canopy water content. The sample size was 69 samples for field grass biophysical data and grass canopy reflectance. Water absorption measures between 1100 and 1250 nm had the highest correlations with above ground biomass, live biomass and canopy water content, while ligno-cellulose absorption measures between 2045 and 2218 nm were the best for estimating senesced biomass. These results suggest possible improvements on estimating grass measures using spectral absorption features derived from hyperspectral sensors. However, relationships were highly influenced by grass species architecture. *B. decumbens*, a more homogeneous, low growing species, had higher correlations between remotely sensed measures and biomass than *B. brizantha*, a more heterogeneous, vertically oriented species. The potential of using the Earth Observing-1 Hyperion data for pasture characterization was assessed and validated using field spectrometer and CCD camera data. Hyperion-derived NPV fraction provided better estimates of grass surface fraction compared to fractions generated from convolved ETM+/Landsat 7 data and minimized the problem of spectral ambiguity between NPV and Soil. The results suggest possible improvement of the quality of land-cover maps compared to maps made using multispectral sensors for the Amazon region.

© 2007 Elsevier Inc. All rights reserved.

**Keywords:** Pasture biophysical characterization; Spectral absorption features; Hyperion; Spectral mixture analysis; Amazon

### 1. Introduction

The spectral properties of vegetation are strongly determined by their biophysical and chemical attributes such as leaf area index (LAI), the amount of live biomass and senesced biomass, moisture content, pigments (e.g., chlorophyll) and spatial arrangement of structures (Asner, 1998; Hill, 2004). Deriving meaningful and accurate measures to quantitatively characterize vegetation still remains a challenge in remote sensing. In part, the accuracy of the retrieval of vegetation properties using

remote sensing depends upon sensor spectral and spatial resolutions. Although broad-band remote sensing has been widely used, this system has limited capability for accurate estimation of vegetation because its coarse spectral resolution leads to ambiguous differentiation between senesced vegetation and soil backgrounds (Roberts et al., 1993; van Leeuwen & Huete, 1996). Hyperspectral remote sensing has the potential of overcoming some of these problems.

Hyperspectral sensors provide a contiguous spectrum defined by a large number of spectral bands, typically measured across the optical wavelengths (350–2500 nm). Improved spectral dimensionality enhances quantification of chemical and physical attributes of vegetation and allows for the development of highly

\* Corresponding author. Tel.: +1 805 893 4434; fax: +1 805 893 3146.

E-mail address: numata@geog.ucsb.edu (I. Numata).

specific spectral indices. For example, spectral absorption features (i.e., absorption depth and area) derived from hyperspectral sensors have been used successfully to estimate foliar biochemistry such as nitrogen, phosphorus, lignin, cellulose, and protein (Curran et al., 2001; Kokaly & Clark, 1999; Mutanga et al., 2004; Pu et al., 2003).

Vegetation spectra in the NIR region have been used to estimate canopy water content and leaf area index (Roberts et al., 1997; Serrano et al., 2000; Sims & Gamon, 2003; Ustin et al., 1998). Such features cannot be measured with multispectral sensors like ETM+/Landsat 7.

Remote sensing of vegetation usually utilizes greenness indices that are sensitive to LAI. For instance, an increase in LAI increases the spectral contrast between the near-infrared and red values of the spectrum, which is the basis for measures such as the Normalized Difference Vegetation Index (NDVI). However, some studies have observed that variation in LAI is more highly correlated to the liquid water content measured by water absorption depth than it is with NDVI (Roberts et al., 1997, 2004).

Unlike LAI, dry plant materials have their greatest effect in the short wavelength infrared (SWIR) region between 2000 and 2400 nm (Asner, 1998; Elvidge, 1990; Roberts et al., 1993),

mainly related to the concentration of ligno-cellulose in dry plant residue (Curran, 1989; Curran et al., 2001; Nagler et al., 2000). The amount of dry or senesced biomass in vegetation plays an important role in estimation of carbon storage and plant stress (Asner et al., 1999). Therefore, accurate vegetation biomass measurement requires the full spectrum including the SWIR so that both live and senesced biomass can be estimated (Ustin et al., 2004). Estimates of live and senesced biomass by hyperspectral data would improve our ability to monitor grazed pastures in the Amazon. The addition of the SWIR region provided by hyperspectral data should also improve land-cover characterization. One of the main limitations of multispectral sensors such as ETM+/Landsat 7 for Amazonian land-cover characterization is that non-photosynthetic vegetation (NPV) such as litter and senesced leaves are not spectrally separable from soil in the visible and near-infrared wavelength region. With hyperspectral data, however, these materials can be differentiated based on ligno-cellulose bands in the SWIR (Asner & Lobell, 2000; Nagler et al., 2000; Roberts et al., 1993).

Currently, there are a variety of hyperspectral sensors available from laboratory to field and satellite scales. These sensors should enhance the characterization and quantification

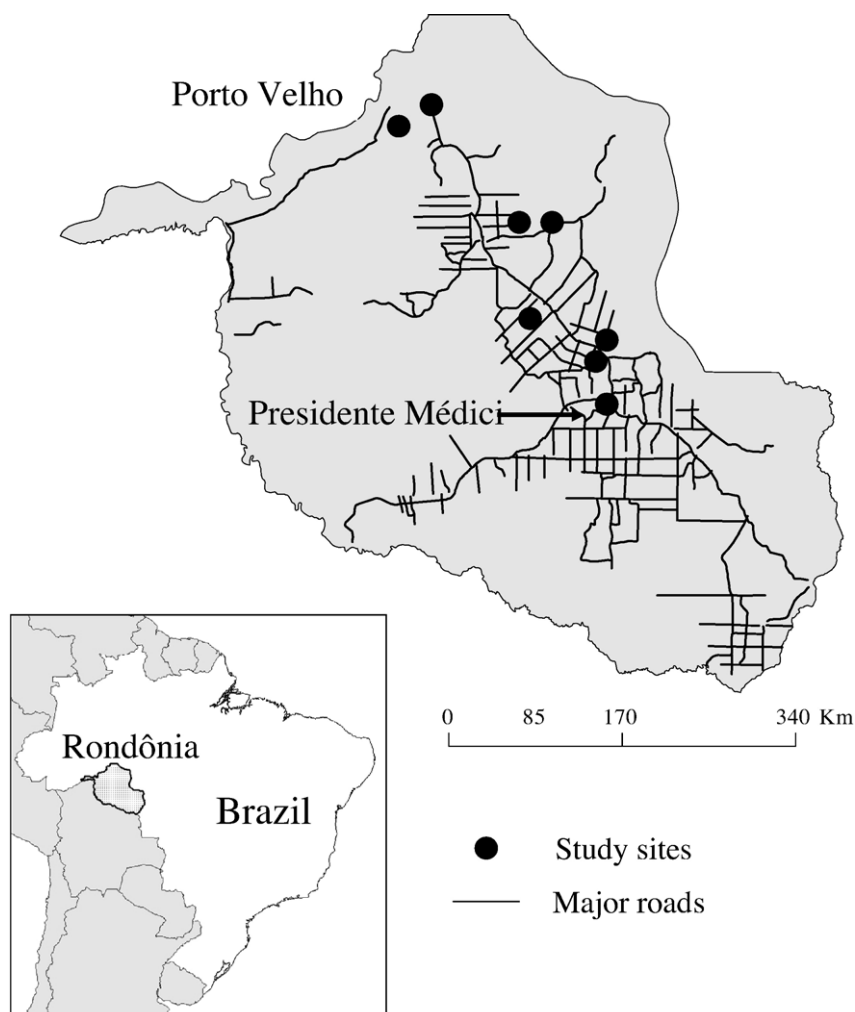


Fig. 1. Study area showing study sites distributed from Porto Velho to Presidente Médici.

of multicomponent pastures and other land-use types in the Amazon. In this study, we investigated the potential for hyperspectral data to improve grazed pasture characterization. There were two specific goals. The first part of this study focuses on evaluating hyperspectrally derived data for estimation of pasture biomass (live, senesced and total biomass) and canopy water content for two grass species at canopy scales using a field spectrometer. The second part addresses the use of the spaceborne hyperspectral sensor, Hyperion, to retrieve pasture composition (i.e., NPV, green vegetation and soil) by

comparison to convolved ETM+/Landsat 7 data, at the local scale, discussing the potential gains from using hyperspectral data relative to a conventional multispectral system.

## 2. Methodology

### 2.1. Study site

The state of Rondônia is located in the southwestern Brazilian Amazon, occupying an area between 8°40' and 15°

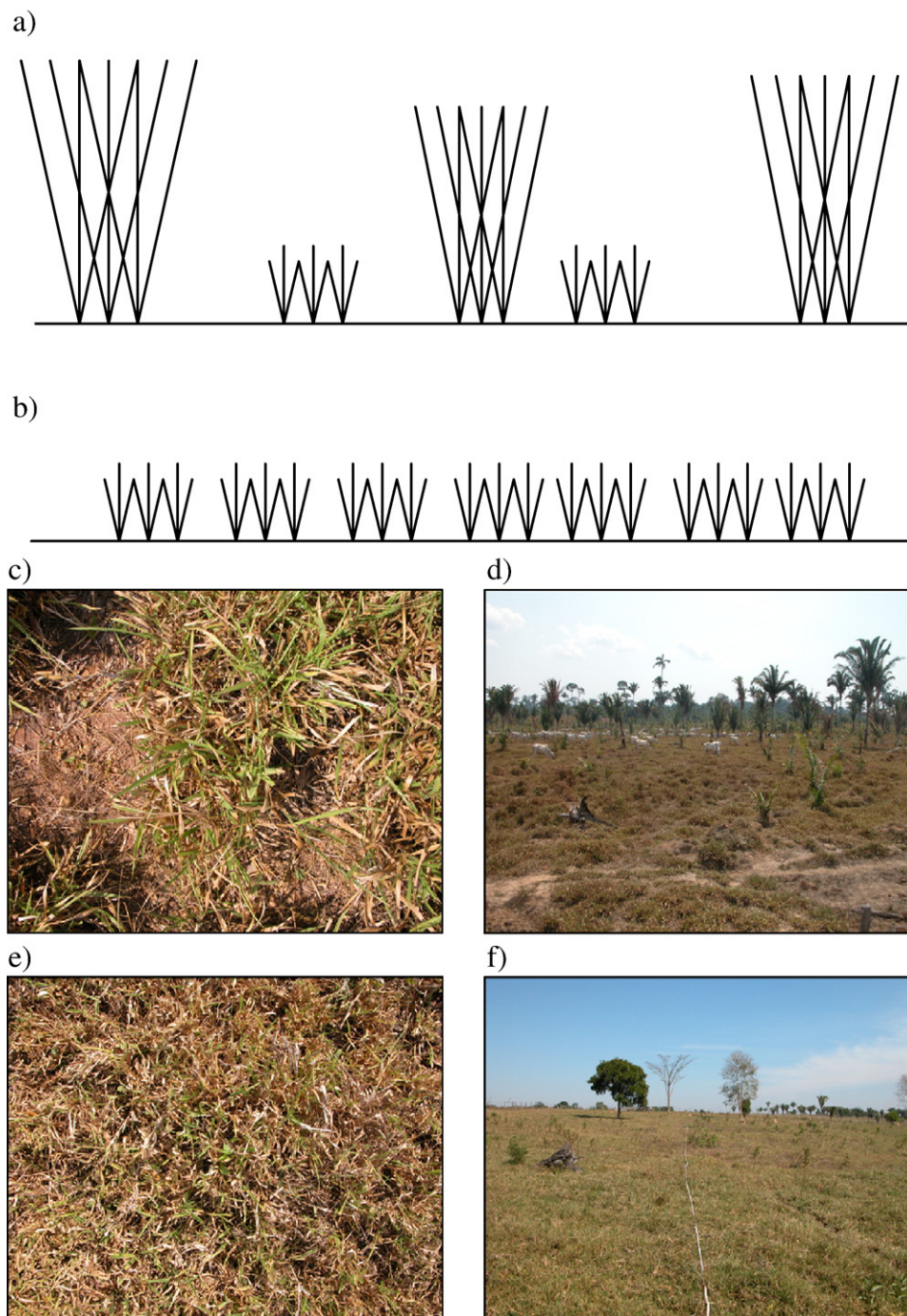


Fig. 2. Grass structures. a) *B. brizantha*, b) *B. decumbens*, c) Canopy of *B. brizantha*, d) overview of *B. brizantha*, e) canopy of *B. decumbens*, and f) overview of *B. decumbens*.

40°S and 60° 22' to 65° 50' W (Fig. 1). Eight ranches were used for this study, distributed in the cities of Porto Velho, Ariquemes, Ouro Preto, Ji-Paraná and Presidente Médici. These ranches are beef and dairy pastures. Soil types are related to geology and topography of this region. Oxisols and Ultisols, both dystrophic soils, are found mostly over the Precambrian granitoid and meta-supracrustal rocks with predominantly flat topography in the north of the state, while Alfisols are distributed mainly in central of Rondônia to the south, where they coincide with the presence of intrusive basic and ultrabasic rocks with gently rolling topography (CPRM, 1997; EMBRAPA, 1983; Holmes et al., 2004).

## 2.2. Part 1: Estimation of pasture biomass and canopy water content with field spectrometer data

Pasture biophysical, i.e., biomass, water content and canopy height, and spectral measurements were obtained from the eight cattle ranches mentioned before. Within each study site, these measures were taken from 100 m transects placed on areas. In total, fourteen transects were used for grass measurements in this study, out of which nine transects consisted of *Brachiaria brizantha*, mostly used for beef pasture, and the rest was of *Brachiaria decumbens*, primarily utilized for dairy pasture (Fig. 2).

### 2.2.1. Field spectral measurements

An Analytical Spectral Device (ASD) – full range spectrometer (350 to 2500 nm, Boulder, CO), on loan from the Jet Propulsion Laboratory (JPL), was used for field optical measurements over transects. The ASD measurements were conducted for all transects. The ASD spectra were collected with a 22° field of view (FOV) with a 1 m sensor height above grass canopies. The spectra were collected at 5 m intervals along each transect initially, however for comparative analysis with grass biophysical data, we used only those spectra collected at the same plots, i.e., at every 20 m intervals along the transects, used for grass biomass sampling. All spectral measurements were collected within 2 h of local solar noon under clear-sky conditions. Five measurements were taken for each grass canopy. These spectra were standardized to spectralon (Lab-sphere, Inc, North Sutton, NH) measured at approximately 10 minute intervals, and converted into reflectance. Averaged reflectance out of five replicate for each grass canopy was used for the analysis. In total, 69 reflectance spectra, which coincided with grass biophysical samples, were used for comparison with the field grass data. The reflectance data were smoothed by a 3 nm window using mean smoothing filter.

### 2.2.2. Biophysical measurements

After collecting grass spectra, standing biomass and litter on the soil surface were collected using a 50 cm × 50 cm quadrat at 20 m intervals along each 100 m transect gathering six biomass samples per transect, and the standing biomass was separated into live and senesced biomass. To avoid mismatch between ASD FOV and 50 cm × 50 cm quadrat of grass biomass measurements, a reference stack was placed at the center of each

measurement plot for biomass clipping after ASD measurements. All grass materials, live, senesced, and litter were weighed soon after clipping and then dried at 70 °C for 36 h. Dried grass materials were weighed again in order to calculate grass water content. During this process, some grass materials were damaged or lost and in total 69 grass samples were remained for the analysis.

### 2.2.3. Data analysis

To analyze which spectral bands and regions of the spectrum are correlated with grass measurements, the first derivative reflectance (FDR) was calculated. FDR indicates the rate of spectral change or slope over an interval of two narrow spectral bands and also normalizes the brightness differences between spectra. FDR was derived from the following equation (Dawson & Curran, 1998)

$$FDR_{\lambda(i)} = (R_{\lambda(j+1)} - R_{\lambda(j)})/\Delta\lambda \quad (1)$$

where FDR is the first derivative reflectance at a wavelength  $i$  midpoint between wavebands  $j$  and  $j+1$ .  $R_{\lambda(j)}$  is the reflectance at waveband  $j$ ,  $R_{\lambda(j+1)}$  is the reflectance at waveband  $j+1$ , and  $\Delta\lambda$  is the difference in wavelengths between  $j$  and  $j+1$ .

A number of spectral indices were calculated and compared with pasture biomass and grass canopy water content (Table 1). The main spectral approach for this study involved the use of spectral absorption features that can be calculated only from hyperspectral data. Two absorption regions in vegetation reflectance were used: 1) water absorption in the range between 1100 and 1250 nm; and 2) lignin and cellulose absorptions in the range between 2045 and 2218 nm for two grass species (Fig. 3). The depth of the spectral absorption around 1200 nm is related to the vegetation water content as well as LAI (Kumar et al., 2001; Roberts et al., 2004; Sims & Gamon, 2003), whereas the depth around 2100 nm is a function of ligno-cellulose concentrations in dry vegetation tissue (Curran, 1989), which may correlate to dry biomass. The depth and the area of these absorption features were calculated using the techniques

Table 1  
Spectral indices used in this study for pasture biomass and canopy water content estimation

Spectral indices/features	Method	Reference
Absorption depth		
1100 and 1250 nm	Continuum removal method	Clark and Roush (1984)
2105 and 2230 nm		
Absorption area		
1100 and 1250 nm	Continuum removal method	Pu et al. (2003)
2105 and 2230 nm	Depth × width of absorption	
Normalized Difference Vegetation Index (NDVI)	(R800 – R680)/(R800 + R680)	Rouse et al. (1973)
Normalized Difference Water Index (NDWI)	(R864 – R1245)/(R864 + R1245)	Gao (1996)
Fractions from linear Spectral Mixture Model (SMA)	Gram Schmidt orthogonalization	Adams et al. (1993)

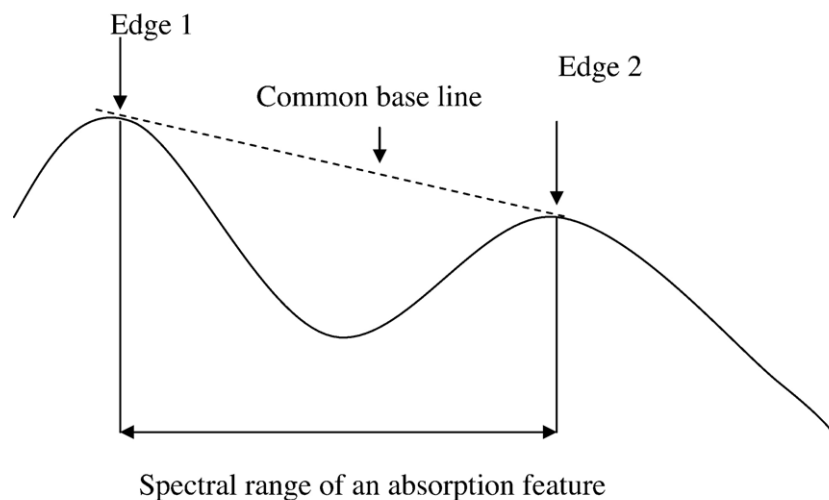
developed by Clark and Roush (1984), Kokaly and Clark (1999) and Pu et al. (2003). These techniques were based on the continuum removal method (Clark & Roush, 1984) that normalizes the spectral curves of the absorption features by establishing a common baseline between the edges of the absorption region (Fig. 3). The absorption depth is a normalized depth of the absorption feature from the common baseline. We used the largest normalized depths in the spectral absorption ranges in this study. The absorption area is the product of absorption depth and the width of absorption which is full wavelength width at half absorption depth.

In addition to the above measures, two vegetation indices, NDVI and Normalized Difference Water Index (NDWI), and fractions from spectral mixture analysis (SMA) were calculated (Table 1). NDVI is sensitive to variation of chlorophyll content and leaf area index (LAI), whereas NDWI is a spectral index sensitive to vegetation water content, and LAI (Gao, 1996). For SMA, a four-endmember model composed of non-photosynthetic

vegetation (NPV), green vegetation (GV), Soil and photometric shade was applied for those plots with exposed soil, and the remaining spectra were unmixed with a three-endmember model, excluding the Soil endmember. Endmembers for these components were selected from a spectral library built from the ASD spectra, which included grasses with different phenological status (e.g., senesced to green leaves), exposed soils, and some green leaves from different vegetation species. Endmembers for these components were selected based on a subset of spectra that produced physically reasonable fractions between 0 and 100% for all components and produced the lowest root mean square error (Roberts et al., 1998). Using this approach, one candidate was selected for each component.

Simple and multiple regressions were used for evaluating pasture biomass and canopy water content estimation from spectral indices. For multiple regression analysis, only two variables were considered. These statistical analyses were accomplished by the R program.

a) A spectral absorption feature with established common line



b) Normalized spectral curve by common base line

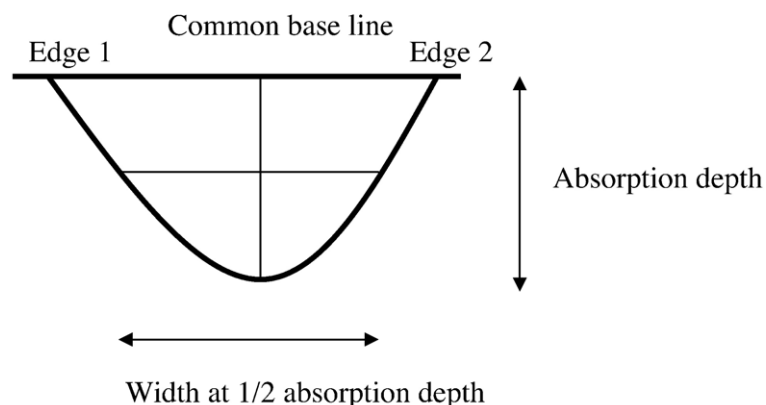


Fig. 3. Illustration of a normalized spectral absorption curve.

### 2.3. Part 2: Characterization of pasture composition with Hyperion and convolved ETM+/Landsat 7 data

#### 2.3.1. Hyperion and data processing

Hyperion is a spaceborne imaging spectrometer consisting of 242 bands ranging from 356 to 2577 nm that acquired data at approximately 10 nm intervals (Pearlman et al., 2003; Ungar et al., 2003). However, only 198 bands were radiometrically calibrated (Datt et al., 2003). The image was acquired on 08/01/2003, which coincided with the field work period. The image has a nominal cross-track swath width of 7.65 km and a downtrack image length of 94 km. The sensor has a nominal ground instantaneous field of view (GIFOV) of 30 m and 12-bit radiometric quantization (Pearlman et al., 2003). The Hyperion image was geometrically registered to our Landsat TM reference data. The Hyperion radiance values from the 198 bands were converted into surface reflectance values, using the Atmospheric Correction Now (ACORN) software which is based on the MODTRAN 4 code. A tropical model was used to minimize scattering and absorption effects of several atmospheric constituents (e.g., water vapor, carbon dioxide, ozone, and oxygen), and visibility, time of day, and the position (lat/long) of scene center were also provided for atmospheric corrections of the image. A column water vapor was fixed at 30 mm while atmosphere visibility was set at 40 km. A minimum noise fraction (MNF) transformation was applied to the surface reflectance image to separate noise from the data (Apan et al., 2004; Datt et al., 2003; Green et al., 1988). The Environment for Visualizing Images — ENVI 4.0 software (ENVI; Research Systems, Boulder, CO) was used for this transformation. There are two steps in this process: forward MNF and inverse MNF. In the first step, a forward MNF estimates noise statistics from the original Hyperion reflectance data and based on the noise statistics, decorrelates and rescales the noise in the data. These results in the MNF transformed data (bands). Next, good bands with less or no noise were selected from the MNF bands. In the final step, the selected MNF bands were transformed back to the original spectral space minimizing noise in the original data.

There is only one study site with three 100 m transects covered by Hyperion data (Lat=9° 51' 25", Lon=62° 40' 00"). This site is a beef pasture ranch with *B. brizantha*. Oxisols are the dominant soil order at this site. To evaluate the potential of Hyperion for pasture characterization, we compared horizontal fractions of NPV, GV and Soil calculated from different sensors (ASD, Hyperion, simulated ETM+/Landsat 7 and the CCD). ASD reflectance measurements and CCD data were collected at 5 m interval along each 100 m transect. In total, 63 measurements for each one of data types, i.e., ASD and CCD were collected from three transects of the study site. Hyperion reflectance data were extracted from three transects ( $n=12$  pixels). ETM+/Landsat 7 convolved reflectance were generated from the Hyperion reflectance using the Landsat spectral response function. SMA was performed for all three datasets, i.e., ASD, Hyperion and ETM+convolved reflectance spectra, in order to compare them.

CCD data were decomposed into GV, Shadow and NPV+Soil. An example of a CCD image decomposed into three

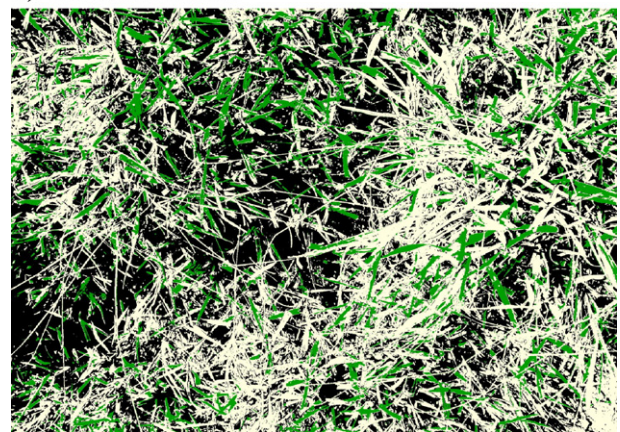
components is shown in Fig. 4. The CCD Shadow was defined by threshold values ranging between 0 and 75 in the red band, while the CCD GV corresponded to non-shadow pixels with a ratio of green to red bands between 1.01 and 5.0. These thresholds were determined empirically. The remaining pixels other than Shadow and GV were defined as NPV+Soil. To separate these two fractions, the CCD Soil amount was visually estimated from the CCD NPV+Soil fraction by using the region of interest (ROI) for soil fraction. Then, from the numbers of pixels of the soil ROIs and other remained pixels in NPV+Soil fractions, we calculated the fractions (percentages) of Soil and NPV, respectively.

Endmembers for NPV, GV and Soil were selected from an ASD field spectral library. CCD fraction data were used as the reference data for ASD, Hyperion and ETM+ convolved spectra. Since the fractions derived from three sensors and the CCD camera are affected by the different illumination effects due to spatial scales, the fractions NPV, GV and Soil

a) CCD



b) Classified CCD



■ Shadow = 40.5 %    □ NPV = 45.5 %  
 ■ GV = 14.0 %

Fig. 4. Illustration of CCD classification of pasture site. Shadow, GV, and NPV fractions were calculated. Soil was virtually interpreted and calculated, when this fraction was in CCD.

Table 2  
Average and standard deviation (parentheses) of pasture biophysical measurements

Species	AGB (g/m <sup>2</sup> )	LB (g/m <sup>2</sup> )	SB (g/m <sup>2</sup> )	WC (g/m <sup>2</sup> )	LB/SB	Height (cm)
<i>B. brizantha</i> (n=46)	562 (275)	435 (240)	127 (73)	211 (115)	3.9	24 (12)
<i>B. decumbens</i> (n=23)	326 (241)	270 (220)	56 (39)	138 (108)	4.9	13 (8)

The abbreviations are: AGB = above ground biomass, LB = live biomass, SB = senesced biomass, WC = water content, LB/SB = live biomass and senesced biomass ratio, and Height = canopy height.

were shade normalized (shadow in the case of CCD data) to minimize illumination problems (Adams et al., 1993).

$$\text{S.N.Fraction} = \frac{\text{Fraction}}{100 - \text{Shade}} \quad (2)$$

### 3. Results and discussion

#### 3.1. Pasture biomass and canopy water content estimation using the field spectrometer

Table 2 shows the biophysical measurements for the two grass species. *B. brizantha* had higher biomass (above ground, live and senesced), water content and canopy height relative to *B. decumbens*, whereas *B. decumbens* had a higher ratio of live to senesced biomass and had a higher proportion of water content in the total biomass (not shown). Both species had similar spectral characteristics (Fig. 5a), but *B. decumbens* spectra had a slightly higher NIR to red contrast. Spectral variability for both species tends to increase from the visible to SWIR (Fig. 5b). *B. brizantha* had greater spectral variability in the visible, NIR, and SWIR1 (1460 to 1730 nm) compared to *B. decumbens*, both showing similar variability in the SWIR2 (2000 to 2400 nm).

Correlograms show the correlations between FDR and grass biomass and water content as a function of wavelengths (Fig. 6). Overall, *B. decumbens* showed higher correlation coefficients than *B. brizantha*. In the correlograms for above ground biomass and water content, high correlations were found at 514 and 580 nm in the visible; 700 nm at the red edge; and in water absorption regions such as 955 nm, 1160 nm and in the SWIR1 (1540 to 1650 nm) for *B. decumbens*. *B. decumbens* has a higher live to senesced biomass ratio and water content (Table 2), and live biomass plays an important role in both grass biomass and canopy reflectance of this species, whereas the FDR of *B. brizantha*, which has lower LB/SB ratio, showed lower correlations in water and chlorophyll absorption regions. In contrast, both species showed similar levels of correlation in the SWIR2 (2000 and 2300 nm). The highest correlations were observed at 2153 and 2213 nm and the latter is the highest in the SWIR for both species ( $r = -0.59$  for *B. brizantha*, and  $r = -0.54$  for *B. decumbens*).

The relationships of pasture biomass and canopy water content with remotely sensed measures for each species and for both species combined are shown in Table 3. The results reveal that the relationships varied strongly as a function of grass species. Overall, *B. brizantha* had lower correlations compared to *B. decumbens*. Since *B. brizantha* dominates 66% of the total samples, the correlations of this species with field measures are similar to the pooled data. For above ground live biomass and water content, water absorption depth and water absorption area between 1100 and 1250 nm had the highest  $r^2$ . Water absorption depth and water absorption area had  $r^2$  values of 0.56 and 0.57, respectively, with above ground biomass for *B. decumbens*. GV and Soil, fractions derived from SMA, were the next measures that showed good relationships with above ground and live biomass, and water content for *B. brizantha*, while *B. decumbens* had high correlations for NPV and GV from SMA. NDVI and NDWI were weakly correlated across all field measures and showed lower correlations than water absorption depth and water absorption area (Table 3 and Fig. 7), indicating that water absorption features derived from hyperspectral sensors can be better measures for estimating pasture

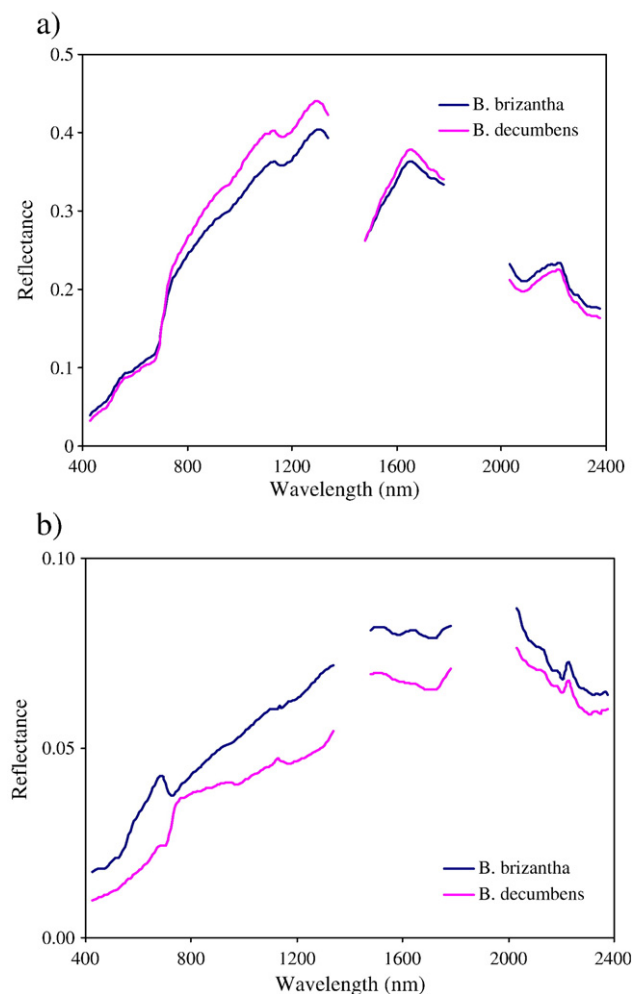


Fig. 5. a) Averaged reflectance for *B. brizantha* and *B. decumbens*. b) Standard deviation values for the two species.

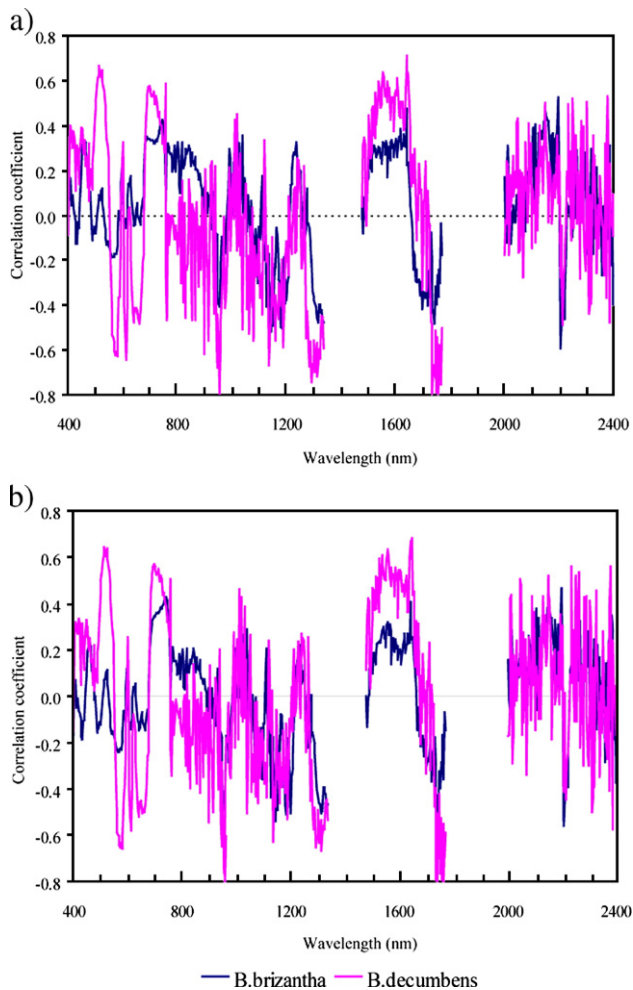


Fig. 6. Correlograms of first derivative reflectance with a) above ground biomass, and b) canopy water content.

biomass compared to spectral vegetation indices such as NDWI and NDVI.

With respect to senesced biomass, the hyperspectral-derived absorption features, ligno-cellulose absorption depth and ligno-cellulose absorption area had the highest  $r^2$  with senesced grass biomass for *B. decumbens* (Table 3). Again, much lower correlations of these indices were found for *B. brizantha*. There is a trend of saturation of water absorption area and ligno-cellulose absorption depth above 200 g/m<sup>2</sup> of senesced biomass observed in *B. brizantha*, and relationships can be better expressed by non-linear trend, especially for *B. brizantha*. Meanwhile, senesced grass biomass of *B. decumbens* that is less than 150 g/m<sup>2</sup> had a strong relationship with ligno-cellulose absorption depth (Fig. 8). This suggests that ligno-cellulose absorption depth provides a better estimate of a lower amount of grass senesced biomass, e.g., <200 g/m<sup>2</sup>. Due to positive relationships between above ground biomass and senesced biomass, water absorption depth and water absorption area were positively correlated with senesced biomass as well. NPV did not perform well for senesced biomass and for *B. decumbens*, NPV showed better relationships with above ground, live biomass and water content, compared to senesced biomass.

Moreover the relationship for NPV is negative (i.e., high NPV for low senesced biomass).

These contrasting results between two species may be primarily related to spatial (horizontal and vertical) heterogeneity of each grass species. *B. brizantha* has stout erect culms forms bunched crowns that create a tufted structure that does not cover the soil surface evenly, resulting in a highly heterogeneous surface (Fig. 2a, c, and d). *B. decumbens* is low growing, more decumbent and forms a dense cover, creating a more homogeneous canopy surface (Fig. 2b, e, and f). Grass reflectance is strongly affected by canopy structural factors

Table 3

Coefficients of determination ( $r^2$ ) calculated from linear regressions for the relationships between pasture biomass and canopy water content and field remotely sensed measures for two grass species

	Remote measures	Combined (n=69)	<i>B. brizantha</i> (n=46)	<i>B. decumbens</i> (n=23)
Above ground biomass	WAD	0.29	0.31	0.56
	WAA	0.31	0.35	0.57
	LCD	0.21	0.21	0.24
	LCA	0.20	0.19	0.13
	NDWI	0.13	0.14	0.32
	NDVI	0.03	0.08	0.36
	NPV	0.01	0.01	0.55
	GV	0.15	0.21	0.50
	Soil	0.08	0.21	0.01
	Shade	0.00	0.01	0.01
Live biomass	WAD	0.30	0.30	0.54
	WAA	0.31	0.31	0.54
	LCD	0.14	0.11	0.12
	LCR	0.13	0.11	0.06
	NDWI	0.14	0.11	0.31
	NDVI	0.05	0.10	0.41
	NPV	0.03	0.0	0.53
	GV	0.18	0.20	0.50
	Soil	0.08	0.16	0.01
	Shade	0.01	0.01	0.02
Senesced biomass	WAD	0.06	0.07	0.24
	WAA	0.08	0.14	0.31
	LCD	0.28	0.25	0.64
	LCA	0.29	0.25	0.57
	NDWI	0.01	0.02	0.01
	NDVI	0.01	0.01	0.01
	NPV	0.01	0.10	0.18
	GV	0.00	0.05	0.09
	Soil	0.02	0.14	0.01
	Shade	0.0	0.06	0.02
Water content	WAD	0.35	0.38	0.45
	WAA	0.36	0.38	0.46
	LCD	0.13	0.09	0.12
	LCA	0.11	0.08	0.06
	NDWI	0.17	0.18	0.22
	NDVI	0.07	0.14	0.31
	NPV	0.04	0.00	0.39
	GV	0.21	0.26	0.40
	Soil	0.09	0.28	0.01
	Shade	0.02	0.00	0.03

WAD = water absorption depth; WAA = water absorption area; LCD = ligno-cellulose absorption depth; LCA = ligno-cellulose absorption area; NDWI = Normalized Difference Water Index; NDVI = Normalized Difference Vegetation Index; NPV = non-photosynthetic vegetation; and GV = green vegetation.

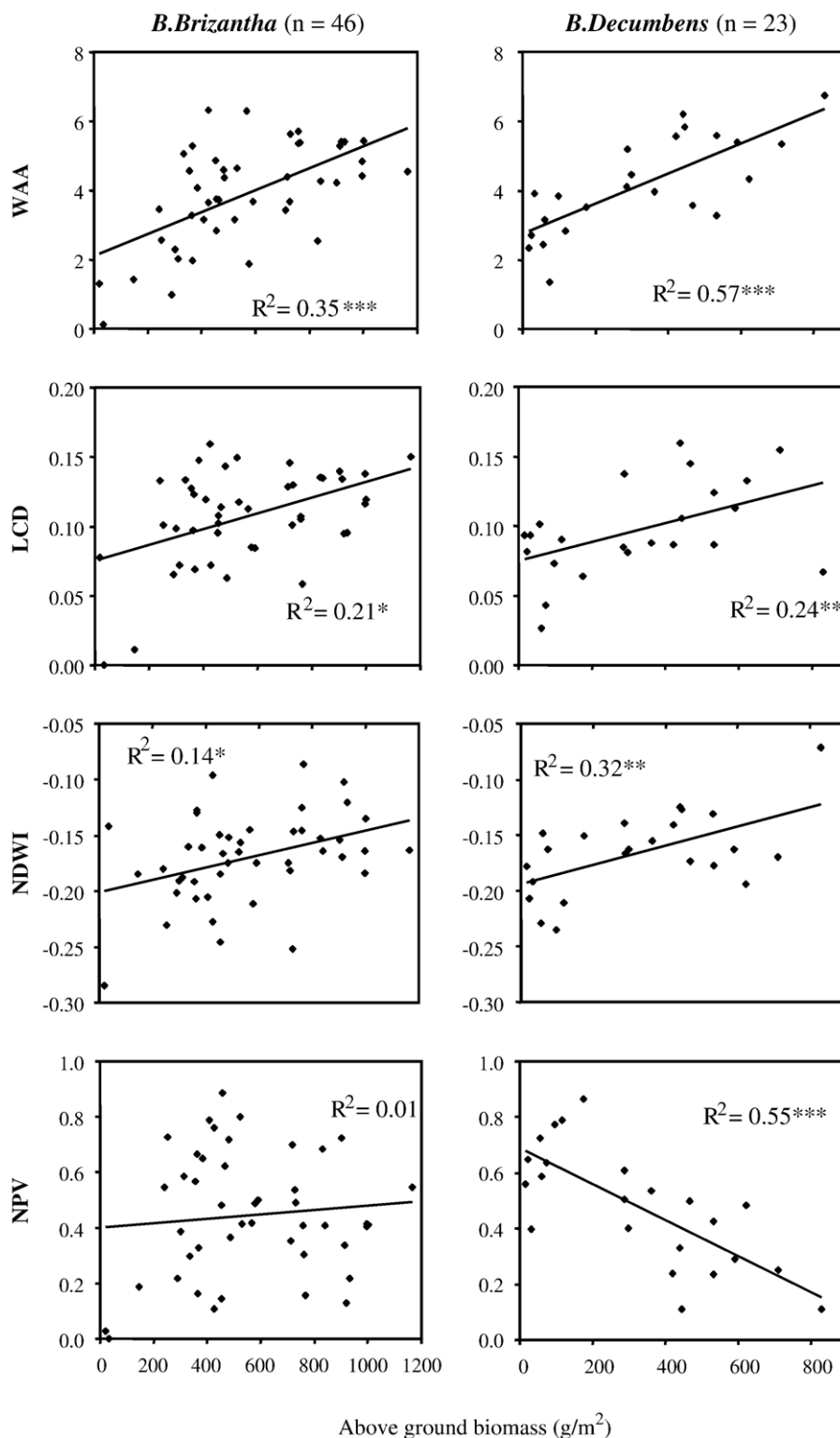


Fig. 7. Scatterplots between above ground biomass and spectral measures derived from ASD, for two grass species, *B. brizantha* and *B. decumbens*. \*\*\* $P < 0.001$ , \*\* $P < 0.01$ , \* $P < 0.05$ , .  $P < 0.1$ .

including leaf area, leaf orientation and angular distributions, density of reflective or absorptive structures and the spatial arrangement of structures. These factors can vary considerably within and between species (Asner, 1998; Hill, 2004). The variation in canopy structures within the field of view of the

ASD sensor contributes to spectral variability of canopy reflectance even for those areas with the same amount of biomass. As a result, the heterogeneous and complex canopy structures of *B. brizantha* make biomass estimation more challenging. Another possible reason for poor relationships is

because mis-registration between grass biophysical data and spectral data. ASD FOV projected on the grass canopy and 50 cm × 50 cm plot for grass biophysical measurements did not perfectly match and many times these two data types collected from the same site were not spatially well calibrated.

In addition to canopy structures, there are other sources of errors or variability in canopy reflectance. Changes in substrate reflectance beneath the grass canopy including soil and litter altered grass reflectance and were more pronounced for areas with low standing biomass. Depending upon the background, i.e., soil or litter, the resulting reflectance can change dramatically. In the case of *B. decumbens*, soil background yields a low ligno-cellulose absorption depth value, while the litter background results in a high ligno-cellulose absorption depth

value. The effects of litter background are more pronounced on NPV of *B. decumbens* (Fig. 8). High ligno-cellulose absorption depth and high NPV values, resulting from the mixture of standing litter and litter on the soil surface, are marked by circles in Fig. 8. The presence of litter on the surface yields very high reflectance over the full-spectral region (400–2500 nm). Moreover, litter has a disproportionately strong effect on canopy reflectance in grasslands where a change in litter biomass plays a much stronger role in driving canopy reflectance variability than a concomitant change in LAI (or any other structural-attributes) (Asner, 1998). NPV appears to be more sensitive to the high reflectance resulting from the litter covered surface compared to the amount of standing biomass or litter.

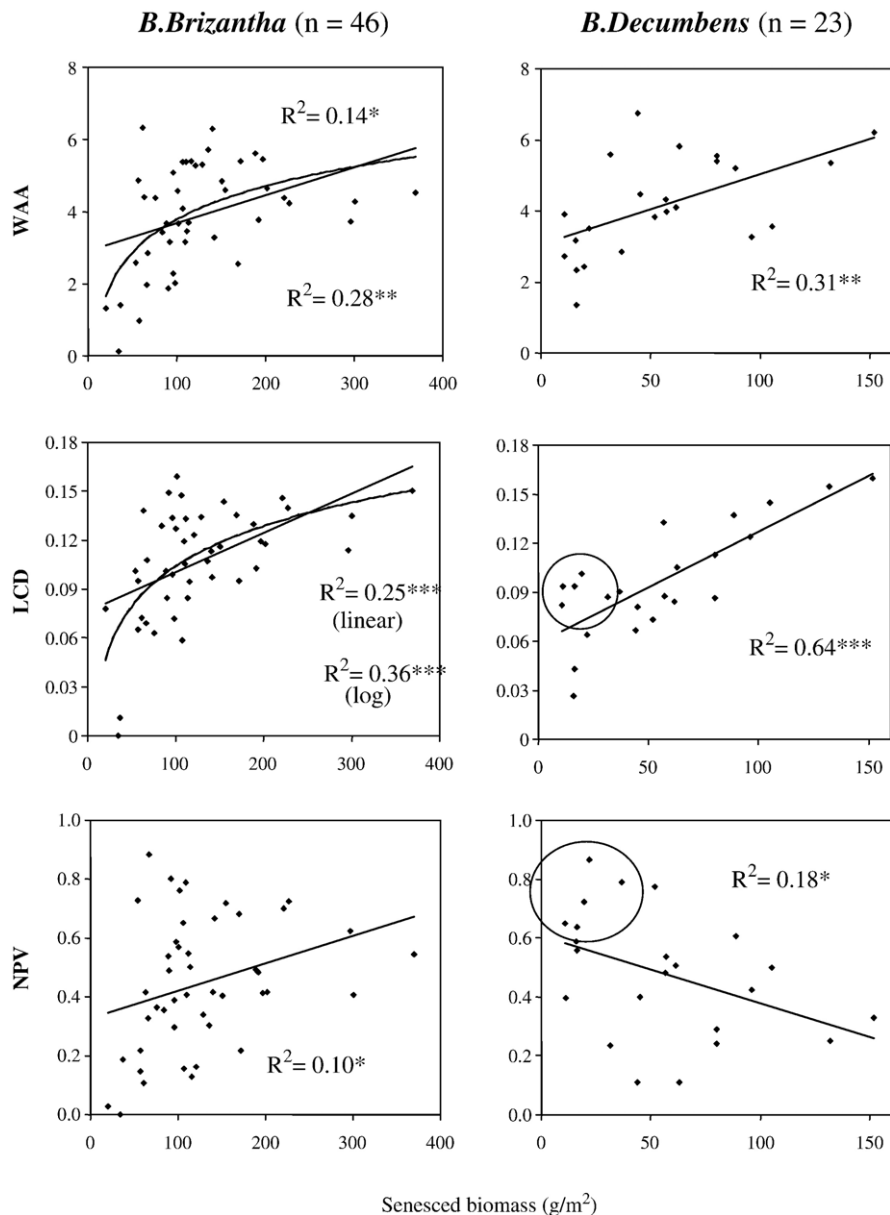


Fig. 8. Scatterplots between senesced biomass and spectral measures derived from ASD, for two grass species, *B. brizantha* and *B. decumbens*. Plots affected by litter background are indicated by circles. \*\*\* $P < 0.001$ , \*\* $P < 0.01$ , \* $P < 0.05$ , .  $P < 0.1$ .

The potential of using two remotely sensed variables was investigated through multiple linear regressions. The best models for each field measure are shown in Table 4. The combinations of water absorption area or water absorption depth with NDVI resulted in the highest correlations and improved the relationships with above ground biomass and live biomass for *B. brizantha*, compared to a single variable, although the correlations were still low. For example, for above ground biomass,  $r^2$  improved from 0.31 to 0.38, from one to two variables. On the other hand, little or no effects of two-variable models were found on the relationships for *B. decumbens*. This indicates that it may be necessary to include more than one remotely sensed measure to characterize a species with more complex canopy structures. For senesced biomass, the combinations of ligno-cellulose absorption area or ligno-cellulose absorption depth with NDWI had the highest correlations. It was expected that the combination of water absorption indices and ligno-cellulose indices, the best indices for live and senesced biomass respectively, would improve the retrieval of above ground biomass of grass. However, little improvement was seen with the water absorption area+ligno-cellulose absorption area model compared to the water absorption area model alone for *B. decumbens*, and no improvement for *B. brizantha*. In the case of *B. brizantha*, for senesced biomass, NDWI is the second explanatory variable used for the best model. Again, this variable performed very poorly for the relationships with field measures for a single variable model, but contributed to improve the relationship in combination with ligno-cellulose absorption depth or ligno-cellulose absorption area.

Hill (2004) summarizes a number of grass/managed pasture vs. remote sensing studies, which had strong relationships between grass biophysical measurements and remotely sensed measures. In general, we had lower correlations and weaker relationships compared to most studies cited in Hill (2004). However he also points out that the relationship between grass biomass and remotely sensed measures holds best for moderate-to-short canopies that contain a high proportion of green, growing material. Since our study was conducted in the dry season, most of grass materials were senesced. This is relatively a unique case that is absent in most grass-remote sensing

studies. In addition, our results showed that the decumbent-short species, *B. decumbens*, had higher  $r^2$  compared to taller species. Taking these points into account, our results are consistent with Hill's observation that the potential of remote sensing for grass characterization is highly influenced by the amount of senesced materials and grass architecture. Therefore, our study provides a unique and important case study among numerous grass-remote sensing studies, showing how the relationships between grass biophysical properties and remotely sensed measures change as a function of species differences (with different architecture) under dry conditions.

Our goal in this study was to investigate the potential of hyperspectral measures to improve pasture characterization. We have found statistically significant relationships between field measurements of biomass and spectral absorption measures derived from hyperspectral data. For example, water absorption features (depth and area) had the best and significant correlations with total biomass and live biomass, and the results were better compared to other measures such as NDWI and NDVI. We found an even stronger relationship for senesced biomass and the depth of ligno-cellulose bands with an  $r^2=0.64$ . These two measures are exactly the ones we might expect to perform best based on physical relationships and neither can be derived from broad-band data.

### 3.2. Characterization of pasture composition with Hyperion and convolved ETM+/Landsat 7 data

Fig. 9 shows the averaged reflectance of grass species *B. brizantha* from the ASD, Hyperion and convolved ETM+ data. The ASD shows a smooth spectrum with some clear absorption features such as chlorophyll (visible), water absorption (near-infrared), and ligno-cellulose (SWIR). Hyperion has a similar spectral shape, but a lower signal to noise compared to the ASD. The convolved ETM+ spectrum has less spectral details compared to the other hyperspectral spectra.

Shade normalized GV, NPV and Soil fractions, derived from the field CCD data were used as the reference data for comparisons between ASD, Hyperion and Landsat data. Shade normalized fractions of different sensors are shown in Table 5. ASD fractions were very close to the CCD fractions, although greater spectral variability (expressed by the standard deviation) was shown in the ASD compared to the CCD measures. The fractional differences between the CCD and Hyperion were greater compared to those between the CCD and ASD, except for the Soil fraction. Despite these results, both the ASD and Hyperion fractions were not statistically different from the CCD ( $t$ -test at 0.95). Landsat overestimated NPV and underestimated GV relative to CCD fractions and these differences were significant ( $t$ -test at 0.95). The Soil fraction was not statistically different from the CCD but it was higher in Landsat. Overall, NPV tended to be overestimated and GV was underestimated by these sensors. The level of accuracy appears to be related to the spectral resolution as well as the signal-to-noise ratio of the sensors. The results indicate that Hyperion has potential for improved estimates of grass properties over conventional multi-spectral systems.

Table 4  
Multiple linear regression models with two remotely sensed variables for pasture biomass and canopy water content estimation

		Model	$r^2$	$P$
Above ground biomass	Both	WAA+NDVI	0.38	<0.0001
	<i>B. brizantha</i>	WAD+NDVI	0.38	<0.0001
	<i>B. decumbens</i>	WAA+NPV	0.60	<0.0001
Live biomass	Both	WAA+NDVI	0.36	<0.0001
	<i>B. brizantha</i>	WAA+NDVI	0.34	<0.0001
	<i>B. decumbens</i>	WAA+NPV	0.58	<0.0001
Senesced biomass	Both	LCA+NDWI	0.34	<0.0001
	<i>B. brizantha</i>	LCA+NDWI	0.31	<0.0001
	<i>B. decumbens</i>	LCA+NDWI	0.70	<0.0001
Water content	Both	WAA+NDVI	0.38	<0.0001
	<i>B. brizantha</i>	WAD+NDVI	0.38	<0.0001
	<i>B. decumbens</i>	WAA+NDVI	0.46	<0.0001

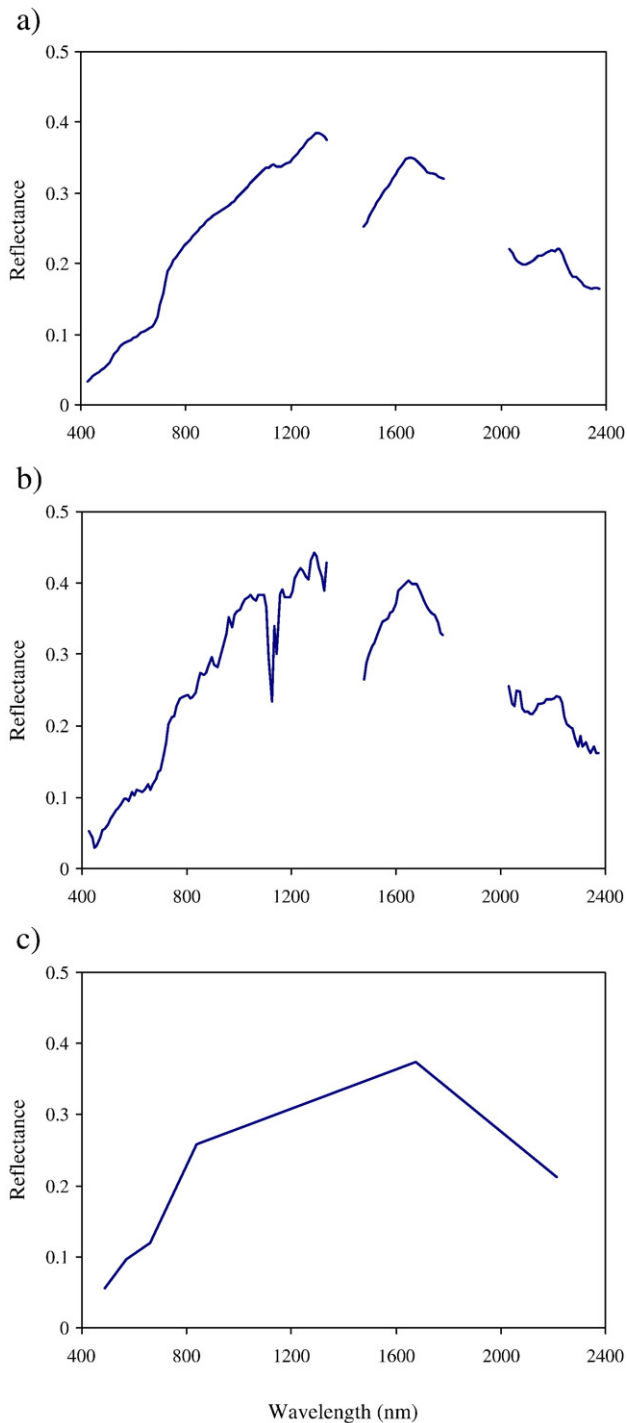


Fig. 9. Averaged reflectance from different sensors: a) ASD, b) Hyperion/EO-1, and c) ETM+/Landsat 7 convolved from Hyperion.

To evaluate potential improvement for pasture analysis by hyperspectral sensors over a multispectral sensor, SMA fractions from Hyperion and convolved ETM+ collected from a wide variety of pasture conditions were compared. Thirty three pasture spectra from the Hyperion image were randomly collected. These spectra cover a range of different pasture status from senesced to green. They were unmixed using the same

endmembers discussed above. The same spectra were convolved to ETM+/Landsat 7 and unmixed and compared to Hyperion fractions. Fig. 10 shows the fractional differences between Hyperion and ETM+ (Hyperion minus ETM+) for each fraction (NPV, GV, Soil and Shade in line) along a gradient from high to low Hyperion GV. There are gaps between the fractions of two sensors. Differences ranged between  $-15$  and  $11\%$  for NPV and between  $-8.6$  and  $8.6\%$  for Soil, whereas differences for GV and Shade fractions were low (less than  $5\%$ ). NPV and Soil are the key to understand the differences between hyper- and multispectral sensors. Hyperion yields substantially higher NPV fractions and lower Soil fractions compared to ETM+ for greener pastures, whereas the opposite trend is found for senesced pastures. A high Soil fraction in green grass is a problem with Landsat. These results indicate that hyperspectral data can reduce this type of error. Therefore, overestimated NPV and lower Soil fractions may be expected for the dry season whereas Soil is overestimated in greener pastures in the wet season from Landsat data.

One of the major sources of errors in this study may be strongly related to scale of field sample size relative to pixel resolution. Our study relied on  $0.5 \text{ m}^2$  field plots to represent a  $30 \text{ m}$  pixel. This sampling scale may be unrepresentative of pasture properties over Landsat pixel. Hill (2004), for example, states that a scale difference between field plots less than  $1.0 \text{ m}^2$  and satellite pixels larger than  $400 \text{ m}^2$  introduces sampling errors into the development of biomass prediction. A higher number of field plots should improve relationships between remotely sensed measures and field data.

The presence of multiple wavelengths in the SWIR region in Hyperion contributes to minimize the problem of spectral ambiguity between NPV and Soil, which is a common problem with broad-band systems. Asner and Heidebrecht (2003) reported that the SWIR2 (2000–2400 nm) provided the most distinctive spectral information for NPV, GV, and Soil for arid regions where vegetation is very sparse. Roberts et al. (2003) verified that Hyperion demonstrated a capability for separating spectral signals from bare soils and senesced plants comparable to the Airborne Visible Infrared Imaging

Table 5

Normalized fractional covers of NPV, GV and Soil for CCD, ASD, Hyperion/EO-1 and convolved ETM+/Landsat 7 spectra from Hyperion

Measurements		Mean	Std. dev.	<i>P</i>
Field measurements (CCD)	NPV	0.81	0.06	–
	GV	0.16	0.05	–
	Soil	0.04	0.07	–
ASD field spectrometer	NPV	0.80	0.17	0.8086
	GV	0.13	0.13	0.3878
	Soil	0.08	0.12	0.2380
Hyperion/EO-1	NPV	0.85	0.11	0.3589
	GV	0.10	0.07	0.1241
	Soil	0.05	0.06	0.8419
ETM+/Landsat 7	NPV	0.94*	0.14	0.0078
	GV	0.07*	0.07	0.0095
	Soil	$-0.01$	0.09	0.1951

Statistically significant mean differences relative to CCD fraction determined using a *t*-test at 0.95 level, are marked with an \*.

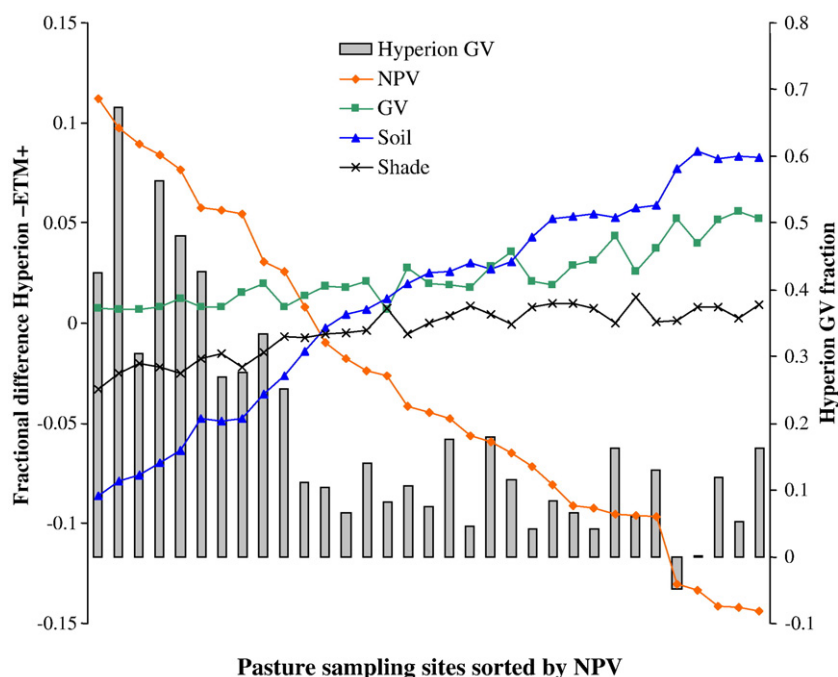


Fig. 10. Fractional differences between Hyperion and convolved ETM+/Landsat 7 from 33 pasture spectra.

Spectrometer (AVIRIS) for Chaparral in Southern California. The enhanced capability for the discrimination of NPV from Soil fractions has been found to be a valuable for land degradation analysis for semi-arid regions (Huete et al., 2003). Furthermore, the spectral information provided from full-spectral range Hyperion data allows us to analyze several spectral vegetation indices for more detailed land-surface characterization of forest phenology, LAI, vegetation species and crops discrimination, and estimation of biochemical properties (Galvão et al., 2005; Gong et al., 2002; Goodenough et al., 2003; Pu et al., 2003). Spaceborne hyperspectral data hold promise for more accurate monitoring for complex land-surfaces in the Amazon region. Although several efforts have been made to classify different land-cover types using Landsat data (Adams et al., 1995; Lucas et al., 1993; Roberts et al., 2002), crops, second growth and green pasture are not spectrally distinct in the broad-band system. This spectral ambiguity can be reduced using hyperspectral data. For grazed pastures in the Amazon region, the potential of retrieving biophysical and biochemical information can be used to study pasture status and its degradation processes.

#### 4. Conclusions

In this study, two hyperspectral sensors at two different spatial scales were tested for grazed pastures in order to investigate the potential for hyperspectral data to improve pasture characterization and (estimates). At canopy scales, hyperspectral absorption features were shown to be the best measures for pasture biomass, i.e., above ground biomass, live biomass, dry biomass and canopy water content. Water absorption features (i.e., water absorption

depth and water absorption area) had the highest correlations with above ground biomass, live biomass, and canopy water content, whereas ligno-cellulose absorption features (i.e., ligno-cellulose absorption depth and ligno-cellulose absorption area) had the highest correlations for senesced biomass. These findings indicate possible improvement for estimating grass measures using spectral absorption features derived from hyperspectral sensors. On the other hand, grass canopy spectra are strongly influenced by canopy architecture and thus pasture biomass and water content estimation is dependent on the grass specie under analysis. Relatively homogeneous *B. decumbens* provided better relationships with spectral measures than *B. brizantha*, a highly heterogeneous surface. More careful field measurements are required to improve the results. The linear combination of spectral variables improved some relationships.

Hyperion provided more accurate biophysical measures for pastures compared to convolved ETM+/Landsat 7 data reducing spectral confusion between NPV and Soil. The results suggest the possibility for improvement of the quality of land-cover maps that have been made by multispectral sensors for the Amazon region. For complex land-surfaces such as grazed pastures, better biophysical and chemical estimates are also expected by using hyperspectral data.

#### Acknowledgements

This study was funded by NASA — grants LBA ECO ND-01 and LBA LC-20. We acknowledge JPL-NASA for loaning the ASD field spectrometer for our field survey. We also greatly thank Francisco Leonidas from EMBRAPA-CPAFRO, Fernando R. Sampaio from Agronomy at UBRA Ji-Paraná, and

João Luiz and Eduardo Lacerda from INCRA Ji-Paraná for technical and logistic support.

## References

- Adams, J. B., Sabol, D. E., Kapos, V., Almeida, R., Roberts, D. A., Smith, M. O., et al. (1995). Classification of multispectral images based on fractions of endmembers — Application to land-cover change in the Brazilian Amazon. *Remote Sensing of Environment*, 52, 137–154.
- Adams, J. B., Smith, M. O., & Johnson, P. E. (1993). Imaging spectroscopy: Interpretation based on spectral mixture analysis. In C. M. Pieters & P. A. J. Englert (Eds.), *Remote Geochemical Analysis: Elemental and Mineralogical Composition* (pp. 145–164). Cambridge, England: Cambridge University Press.
- Apan, A., Held, A., Phinn, S., & Markley, J. (2004). Detecting sugarcane ‘orange rust’ disease using EO-1 Hyperion hyperspectral imagery. *International Journal of Remote Sensing*, 25, 489–498.
- Asner, G. P. (1998). Biophysical and biochemical sources of variability in canopy reflectance. *Remote Sensing of Environment*, 64, 234–253.
- Asner, G. P., & Heidebrecht, K. B. (2003). Imaging spectroscopy for desertification studies: Comparing AVIRIS and EO-1 Hyperion in Argentina drylands. *IEEE Transactions on Geoscience and Remote Sensing*, 41, 1283–1296.
- Asner, G. P., & Lobell, D. B. (2000). A biogeophysical approach for automated SWIR unmixing of soils and vegetation. *Remote Sensing of Environment*, 74, 99–112.
- Asner, G. P., Townsend, A. R., & Bustamante, M. M. C. (1999). Spectrometry of pasture condition and biogeochemistry in the Central Amazon. *Geophysical Research Letters*, 26, 2769–2772.
- Clark, R. N., & Roush, T. L. (1984). Reflectance spectroscopy: Quantitative analysis techniques for remote sensing applications. *Journal of Geophysical Research*, 89, 6329–6340.
- CPRM (1997). *Mapa Geológico do Estado de Rondônia*. RO: Porto Velho.
- Curran, P. J. (1989). Remote-sensing of foliar chemistry. *Remote Sensing of Environment*, 30, 271–278.
- Curran, P. J., Dungan, J. L., & Peterson, D. L. (2001). Estimating the foliar biochemical concentration of leaves with reflectance spectrometry testing the Kokaly and Clark methodologies. *Remote Sensing of Environment*, 76, 349–359.
- Datt, B., McVicar, T. R., van Niel, T. G., Jupp, D. L. B., & Perlman, J. S. (2003). Preprocessing EO-1 Hyperion hyperspectral data to support the application of agricultural indexes. *IEEE Transactions on Geoscience and Remote Sensing*, 41, 1246–1259.
- Dawson, T. P., & Curran, P. J. (1998). A new technique for interpolating the reflectance red edge position. *International Journal of Remote Sensing*, 19, 2133–2139.
- Elvidge, C. D. (1990). Visible and near-infrared reflectance characteristics of dry plant materials. *International Journal of Remote Sensing*, 11, 1775–1795.
- EMBRAPA (1983). *Mapa de levantamento de reconhecimento de meia intensidade dos solos do estado de Rondônia, 1:500.000*. Porto Velho: Comissão Estadual de Planejamento Agrícola.
- Galvão, L. S., Formaggio, A. R., & Tisot, D. A. (2005). Discrimination of sugarcane varieties in southeastern Brazil with EO-1 Hyperion data. *Remote Sensing of Environment*, 94, 523–534.
- Gao, B. C. (1996). NDWI — A normalized difference water index for remote sensing of vegetation liquid water from space. *Remote Sensing of Environment*, 58, 257–266.
- Gong, P., Pu, R., & Heald, R. C. (2002). Analysis of *in situ* hyperspectral data for nutrient estimation of giant sequoia. *International Journal of Remote Sensing*, 23, 1827–1850.
- Goodenough, D. G., Dyk, A., Niemann, O., Pearlman, J. S., Chen, H., Han, J., et al. (2003). Processing Hyperion and ALI for forest classification. *IEEE Transactions on Geoscience and Remote Sensing*, 41, 1321–1331.
- Green, A. A., Berman, M., Switzer, P., & Craig, M. D. (1988). A transformation for ordering multispectral data in terms of image quality with implications for noise removal. *IEEE Transactions on Geoscience and Remote Sensing*, 26, 65–74.
- Hill, M. J. (2004). Grazing agriculture: Managed pasture, grassland, and rangeland. In S. L. Ustin (Ed.), *Manual of Remote Sensing volume 4 Remote sensing for natural resource management and environmental monitoring* (pp. 449–530). Hoboken, NJ: John Wiley & Sons.
- Holmes, K. W., Roberts, D. A., Sweeney, S., Numata, I., Matricardi, E., Biggs, T. W., et al. (2004). Soil databases and the problem of establishing regional biogeochemical trends. *Global Change Biology*, 10, 796–814.
- Huete, A. R., Miura, T., & Gao, X. (2003). Lands cover conversion and degradation analyses through coupled soil–plant biophysical parameters derived from hyperspectral EO-1 Hyperion. *IEEE Transactions on Geoscience and Remote Sensing*, 41, 1268–1276.
- Kokaly, R. F., & Clark, R. N. (1999). Spectroscopic determination of leaf biochemistry using band-depth analysis of absorption features and stepwise multiple linear regression. *Remote Sensing of Environment*, 67, 267–287.
- Kumar, L., Schemid, K., Dury, S., & Skidmore, A. (2001). Imaging spectrometry and vegetation science. In F. D. van Der Meer & S. M. de Jong (Eds.), *Imaging spectrometry: Basic principles and prospective applications*. Dordrecht: Kluwer Academic Publishers.
- Lucas, R., Honzak, M., Foody, G. M., Curran, P. J., & Corves, C. (1993). Characterizing tropical secondary forests using multi-temporal Landsat sensor imagery. *International Journal of Remote Sensing*, 14, 3061–3067.
- Mutanga, O., Skidmore, A. K., & Prins, H. H. T. (2004). Predicting *in situ* pasture quality in the Kruger National Park, South Africa, using continuum-removed absorption features. *Remote Sensing of Environment*, 89, 393–408.
- Nagler, P. L., Daughtry, C. S. T., & Goward, S. N. (2000). Plant litter and soil reflectance. *Remote Sensing of Environment*, 71, 207–215.
- Pearlman, J. S., Barry, P. S., Segal, C. C., Shepanski, J., Beiso, D., & Carman, S. L. (2003). Hyperion, a space-based imaging spectrometer. *IEEE Transactions on Geoscience and Remote Sensing*, 41, 1160–1173.
- Pu, R. L., Gong, P., Biging, G. S., & Larrieu, M. R. (2003). Extraction of red edge optical parameters from Hyperion data for estimation of forest leaf area index. *IEEE Transactions on Geoscience and Remote Sensing*, 41, 916–921.
- Roberts, D. A., Batista, G., Pereira, J. L. G., Waller, E., & Nelson, B. (1998). Change identification using multitemporal spectral mixture analysis: Applications in eastern Amazônia. In C. Elvidge & R. Lunetta (Eds.), *Remote Sensing Change Detection: Environmental Monitoring Applications and Methods* (pp. 137–161). Ann Arbor: Ann Arbor Press.
- Roberts, D. A., Dennison, P. E., Gardner, M. E., Hetzel, Y., Ustin, S. L., & Lee, C. T. (2003). Evaluation of the potential of Hyperion for fire danger assessment by comparison to the Airborne Visible/Infrared Imaging Spectrometer. *IEEE Transactions on Geoscience and Remote Sensing*, 41, 1297–1310.
- Roberts, D. A., Green, R. O., & Adams, J. B. (1997). Temporal and spatial patterns in vegetation and atmospheric properties from AVIRIS. *Remote Sensing of Environment*, 62, 223–240.
- Roberts, D. A., Numata, I., Holmes, K., Batista, G., Krug, T., Monteiro, A., et al. (2002). Large area mapping of land-cover change in Rondonia using multitemporal spectral mixture analysis and decision tree classifiers. *Journal of Geophysical Research—Atmospheres*, 107, 40–41. 40–18.
- Roberts, D. A., Smith, M. O., & Adams, J. B. (1993). Green vegetation, nonphotosynthetic vegetation, and soils in Aviris data. *Remote Sensing of Environment*, 44, 255–269.
- Roberts, D. A., Ustin, S. L., Ogunjemiyo, S., Greenberg, J., Dobrowski, S. Z., Chen, J. Q., et al. (2004). Spectral and structural measures of northwest forest vegetation at leaf to landscape scales. *Ecosystems*, 7, 545–562.
- Rouse, J. W., Haas, R. H., Schell, J. A., & Deering, D. W. (1973). Monitoring vegetation systems in the Great Plains with ERTS. *Proceedings of the third ERTS symposium* (pp. 309–317).
- Serrano, L., Ustin, S., Roberts, D. A., Gamon, J. A., & Peñelas, J. (2000). Deriving water content of chaparral vegetation from AVIRIS data. *Remote Sensing of Environment*, 74, 570–581.
- Sims, D. A., & Gamon, J. A. (2003). Estimation of vegetation water content and photosynthetic tissue area from spectral reflectance: A comparison of indices based on liquid water and chlorophyll absorption features. *Remote Sensing of Environment*, 84, 526–537.

- Ungar, S. G., Pearlman, J. S., Mendenhall, J. A., & Reuter, D. (2003). Overview of the Earth Observing One (EO-1) mission. *IEEE Transactions on Geoscience and Remote Sensing*, *41*, 1149–1159.
- Ustin, S. L., Roberts, D. A., Gamon, J. A., Asner, G. P., & Green, R. O. (2004). Using imaging spectroscopy to study ecosystem processes and properties. *Bioscience*, *54*, 523–534.
- Ustin, S., Roberts, D. A., Pinzón, J., Jacquemoud, S., Gardner, M., Sheer, G., et al. (1998). Estimating canopy water content of chaparral shrubs using optical methods. *Remote Sensing of Environment*, *65*, 280–291.
- van Leeuwen, W. J. D., & Huete, A. R. (1996). Effects of standing litter on the biophysical interpretation of plant canopies with spectral indices. *Remote Sensing of Environment*, *55*, 123–138.